JOURNAL OF MATERIALS PROCESSING TECHNOLOGY 197 (2008) 408–418

journal homepage: www.elsevier.com/locate/jmatprotec

Thermo-mechanical models of steel solidification based on two elastic visco-plastic constitutive laws

Seid Koric[a,*], *Brian G. Thomas*[b]

[a] *National Center for Supercomputing Applications-NCSA, University of Illinois at Urbana-Champaign, 1205 W. Clark Street, Urbana, IL 61801, United States*

[b] *Mechanical Science and Engineering Department, University of Illinois at Urbana-Champaign, 1206 W. Green Street, Urbana, IL 61801, United States*

ARTICLE INFO

Article history:
Received 9 April 2007
Received in revised form 2 June 2007
Accepted 15 June 2007

Keywords:
Thermo-mechanical processes
Solidification and melting
Elastic-visco-plastic material
Finite elements
Constitutive models
Steel casting

ABSTRACT

Two thermo-mechanical models based on different elastic-visco-plastic constitutive laws are applied to simulate temperature and stress development of a slice through the solidifying shell of 0.27%C steel in a continuous casting mold under typical commercial operating conditions with realistic temperature dependant properties. A general form of the transient heat equation, including latent-heat from phase transformations such as solidification and other temperature-dependent properties, is solved numerically for the temperature field history. The resulting thermal stresses are solved by integrating the elastic-visco-plastic constitutive laws of Kozlowski [P.F. Kozlowski, B.G. Thomas, J.A. Azzi, H. Wang, Simple constitutive equations for steel at high temperature, Metall. Trans. 23A (1992) 903–918] for austenite in combination with the Zhu power-law [H. Zhu, Coupled thermal–mechanical finite-element model with application to initial solidification, PhD thesis, University of Illinois, 1993] for delta-ferrite with ABAQUS [ABAQUS Inc., User Manuals v6.6, 2006] using a user-defined subroutine UMAT [S. Koric, B.G. Thomas, Efficient thermo-mechanical model for solidification processes, Int. J. Num. Meth. Eng. 66 (2006) 1955–1989], and the Anand law for steel [L. Anand, Constitutive equations for the rate dependant deformation of metals at elevated temperatures, ASME J. Eng. Mater. Technol. 104 (1982) 12–17; S.B. Brown, K.H. Kim, L. Anand, An internal variable constitutive model for hot working of metals, Int. J. Plasticity 6 (1989) 95–130] using the integration scheme recently implemented in ANSYS [ANSYS Inc., User Manuals v100, 2006]. The results from these two approaches are compared and CPU times are benchmarked. A comparison of one-dimensional constitutive behavior of these laws with experimental tensile test data [P.J. Wray, Plastic deformation of delta-ferritic iron at intermediate strain rates, Metall. Trans. A 7A (1976) 1621–1627; P.J. Wray, Effect of carbon content on the plastic flow of plain carbon steel at elevated temperatures, Metall. Trans. A 13 (1982) 125–134] and previous work [A.E. Huespe, A. Cardona, N. Nigro, V. Fachinotti, Visco-plastic constitutive models of steel at high temperature, J. Mater. Process. Technol. 102 (2000) 143–152] shows reasonable agreement for both models, although the Kozlowski–Zhu approach is much more accurate for low carbon steels. The thermo-mechanical models studied here are useful for efficient and accurate analysis of steel solidification processes using convenient commercial software.

Published by Elsevier B.V.

* *Corresponding author*. Tel.: +1 217 265 8410.
E-mail address: skoric@ncsa.uiuc.edu (S. Koric).
0924-0136/$ – see front matter. Published by Elsevier B.V.
doi:10.1016/j.jmatprotec.2007.06.060

Nomenclature

a	Anand strain rate sensitivity of hardening or softening
A	surface (m^2)
A_A	Anand pre-exponential factor (s^{-1})
A_h	convection-prescribed surface (m^2)
A_q	flux-prescribed surface (m^2)
A_T	temperature-prescribed surface (m^2)
A_u	displacement-prescribed surface (m^2)
A_Φ	traction-prescribed surface (m^2)
$\mathbf{b}$	volumetric force vector (N)
c_p	specific heat (J/kg K)
$\underline{\underline{\mathbf{D}}}$	fourth order elasticity tensor (N/m^2)
E	elastic modulus (N/m^2)
f	visco-plastic law function (s^{-1})
fc	empirical constant in Kozlowski III law ($MPa^{-f3}\,s^{-1}$)
f_1	empirical constant in Kozlowski III law (MPa)
f_2	empirical constant in Kozlowski III law
f_3	empirical constant in Kozlowski III
$f_{\delta c}$	empirical constant in enhanced power delta law
h	general film coefficient ($W/m^2\,K$)
h_o	Anand hardening/softening constant (N/m^2)
H	enthalpy (J/kg K)
Hf	latent heat (J/kg K)
$\mathbf{I}$	second order identity tensor
$\underline{\underline{\mathbf{I}}}$	fourth order identity tensor
k	thermal conductivity (W/m K)
k_B	bulk modulus (N/m^2)
L	characteristic axial casting length (m)
m	Anand strain rate sensitivity of stress; empirical constants used power delta law
n	Anand strain rate sensitivity of saturation; empirical constants used power delta law
$\mathbf{n}$	surface unit vector
$\hat{q}$	prescribed heat flux (W/m^2)
Q, Q_A	activation energy constants (K)
s	Anand deformation resistance (N/m^2)
$\tilde{s}$	Anand saturation value for s (N/m^2)
s_o	Anand initial value for s (N/m^2)
T	temperature (°C, K)
T_{init}	initial temperature (°C)
T_{liq}	liquidus temperature (°C)
T_{sol}	solidus temperature (°C)
T_0	reference temperature (°C)
T_∞	ambient temperature (°C)
TLE	thermal linear expansion
$\hat{T}$	prescribed BC temperature (°C)
$\mathbf{u}$, $\mathbf{d}$	displacement vector (m)
V	volume (m^3)
V_c	casting speed (m/min)
$\mathbf{x}$	position vector (m)
z	distance below meniscus (m)

Greek letters

α	coefficient of thermal expansion ($°C^{-1}$)
δ_{ij}	Kronecker's delta
$\boldsymbol{\varepsilon}$	total strain tensor
$\boldsymbol{\varepsilon}_{\mathbf{el}}$	elastic strain tensor
$\boldsymbol{\varepsilon}_{\mathbf{ie}}$	inelastic strain tensor
$\dot{\boldsymbol{\varepsilon}}$	total strain rate tensor (s^{-1})
$\dot{\boldsymbol{\varepsilon}}_{\mathbf{el}}$	elastic strain rate tensor (s^{-1})
$\dot{\boldsymbol{\varepsilon}}_{\mathbf{ie}}$	inelastic strain rate tensor (s^{-1})
$\dot{\bar{\varepsilon}}_{ie}$	equivalent inelastic strain (s^{-1})
$\boldsymbol{\varepsilon}_{th}$	thermal strain tensor
$\dot{\boldsymbol{\varepsilon}}_{th}$	thermal strain rate tensor (s^{-1})
μ	shear modulus (N/m^2)
ξ	Anand multiplier of stress
ρ	density (kg/m^3)
$\boldsymbol{\sigma}$	stress tensor—small strain formulation (N/m^2)
$\boldsymbol{\sigma}'$	deviatoric stress tensor (N/m^2)
$\bar{\boldsymbol{\sigma}}$	equivalent stress (N/m^2, MPa)
$\boldsymbol{\sigma}^*$	trial stress tensor (N/m^2)
$\boldsymbol{\Phi}$	surface traction vector (N/m^2)
%C	percentage carbon in the steel

1. Introduction

Many manufacturing and fabrication processes such as foundry shape casting, continuous casting and welding have common solidification phenomena. Probably one of the most important and complex among these is continuous casting, which is used to produce over 90% of the steel in the world today. Although the quality of continuous-cast steel is constantly improving, there is always incentive to lower the amount of defects and to improve productivity. Many of the more important defects that plague the continuous casting process are cracking problems. Many of these cracking problems are related to mismatch between solidification shrinkage and mold taper, that causes interfacial gaps and reduced heat flow between the shell and mold, leading to locally hot and thin parts of shell. These often cause transverse stresses, leading to longitudinal cracks at the meniscus, and breakouts due to ferrostatic pressure from the liquid phase applied to the newly solidified shell at mold exit (Li and Thomas, 2002a,b).

Many of these phenomena occur during the early stages of solidification in the mold. Accurate determination of temperature, deformation and stress distributions during this time is important for correct prediction of the taper to avoid these cracking problems, in addition to understanding other cracks, surface defects, and quality problems in the continuous casting of steel and other processes.

The high cost of plant experiments under the harsh operating steel plant conditions makes it appropriate to use all available methods in simulating, optimizing, and designing this process. Although continuous casting has been subject to many computational models, the complexity of the phenomena, including temperature, strain-rate, and phase-transformation-dependent constitutive behavior, make it difficult to model accurately. Improvements to the process to avoid cracks, such as optimizing mold taper designs, demand quantitative models that can make accurate predictions of thermal stress and strain during solidification.

The constitutive models used in previous work to investigate thermal stresses during continuous casting first adopted simple elastic–plastic laws (Weiner and Boley, 1963; Grill et al., 1976; Wimmer et al., 1996). Later, separate creep laws were added (Rammerstrofer et al., 1979; Kristiansson, 1984). With the rapid advance of computer hardware, more computationally challenging elastic-visco-plastic models have been used (Zhu, 1993; Koric and Thomas, 2006; Boehmer et al., 1998; Farup and Mo, 2000; Li and Thomas, 2005; Risso et al., 2006) which treat the phenomena of creep and plasticity together since only the combined effect is measurable. Most previous models adopt a Langrangian description of this process with a fixed mesh, although an alternative mechanical model based on Eularian–Langrangian description has been proposed recently (Huespe et al., 2000; Risso et al., 2006). Similarly, the integration of visco-plastic laws ranges from easy-to-implement explicit methods (Morgan et al., 1978; Lewis et al., 1996), to robust but complex implicitly based algorithms (Zhu, 1993; Koric and Thomas, 2006; Huespe et al., 2000; Li and Thomas, 2005).

It is a considerable challenge to apply these previous in-house FE models to solve realistic problems, which demand the incorporation of other important phenomena such as contact, thermal–mechanical coupling, and three-dimensional complexities. On the other hand, the easy-to-use commercial finite-element packages are now fully capable of handling these related phenomena, having rich element libraries, fully imbedded pre- and post-processing capabilities, advanced modeling features such as contact algorithms, and can take full advantage of parallel-computing capabilities.

The work of Koric and Thomas (2006, 2007) and Koric et al. (2007) implemented a robust local visco-plastic integration schemes from an in-house code CON2D (Zhu, 1993; Li and Thomas, 2002a,b, 2005) into the commercial finite element package ABAQUS via its user defined material subroutine UMAT including the special treatment of liquid/mushy zone. This opened the door for the realistic computational modeling of complex steel solidification processes with ABAQUS (Koric et al., 2007; Koric and Thomas, 2007) based on the Kozlowski III visco-plastic law for austenite, and the Zhu enhanced power law for delta-ferrite phase (Zhu, 1993). The thermal–mechanical predictions of this model were based on measured tensile-test and creep data and have been rigorously validated against analytical solutions, a reliable in-house code (Koric and Thomas, 2006), and with plant measurements (Koric et al., 2007).

Another finite-element commercial package ANSYS has recently implemented a different visco-plastic material, originally proposed by Anand (1982) and Brown et al. (1989) for the hot working of metals. Huespe et al. (2000) compared these two visco-plastic constitutive models of steel and concluded that the Kozlowski model was slightly more accurate and convenient than the Anand model. However, that study considered only one steel carbon content, used an in-house code with limited features and availability, and did not compare execution times.

The object of this article is to compare temperature and stress results from the Anand material model in ANSYS against those of the Kozlowski/Zhu material model using ABAQUS. In this work, a real world simulation of a typical continuous casting process is performed with both codes using realistic temperature-dependant properties on a simple slice domain. To enable a fair comparison of the crucial thermo-mechanical results developing during steel solidification using the different constitutive models, other important phenomena such as complex mold geometries, contact between the mold and strand with gap dependant conductivity, ferrostatic pressure, mold taper etc. are avoided in this paper, although they are being modeled with both of these general purpose codes in related work.

2. Thermal governing equations

Using an uncoupled approach, the heat conduction equation is solved first in a fixed-mesh domain that initially contains only liquid. The resulting temperature solution is then input to the subsequent mechanical analysis. The local form of the transient energy equation is given in Eq. (1) (Lewis et al., 1996):

$$\rho\left(\frac{\partial H(T)}{\partial t}\right) = \nabla\cdot(k(T)\nabla T) \tag{1}$$

along with boundary conditions:

$$\begin{aligned}&\text{Prescribed temperature on } A_T: \quad T = \hat{T}(\mathbf{x},t);\\ &\text{prescribed surface flux on } A_q: \quad (-k\nabla T)\cdot\mathbf{n} = \hat{q}(\mathbf{x},t);\\ &\text{surface convection on } A_h: \quad (-k\nabla T)\cdot\mathbf{n} = h(T-T_\infty)\end{aligned} \tag{1a}$$

where ρ is the density, k the isotropic temperature dependant conductivity, H is temperature dependant enthalpy, which includes the latent heat of solidification. $\hat{T}$ is a fixed temperature at the boundary A_T, $\hat{q}$ the prescribed heat flux at the boundary A_q, h the film convection coefficient prescribed at the boundary A_h where T_∞ is the ambient temperature, and $\mathbf{n}$ is the unit normal vector of the surface of the domain.

3. Mechanical governing equations

The strains which dominate thermo-mechanical behavior during solidification are on the order of only a few percent, or cracks will form (Thomas et al., 1986). Thus, the assumption of small strain is adopted in this work. Several previous solidification models (Zhu, 1993; Kristiansson, 1984; Li and Thomas, 2005; Risso et al., 2006) confirm that the solidified metal undergoes only small deformation during initial solidification in the mold. With displacement spatial gradient, $\nabla\mathbf{u} = \partial\mathbf{u}/\partial\mathbf{x}$ being small, $\nabla\mathbf{u}{:}\nabla\mathbf{u} \approx 1$ and the linearized strain tensor is thus (Mase and Mase, 1999)

$$\boldsymbol{\varepsilon} = \frac{1}{2}[\nabla\mathbf{u} + (\nabla\mathbf{u})^T] \tag{2}$$

where Cauchy stress tensor is identified with the nominal stress tensor $\boldsymbol{\sigma}$, and $\mathbf{b}$ is the body force density with respect to initial configuration:

$$\nabla\cdot\boldsymbol{\sigma}(\mathbf{x}) + \mathbf{b} = 0 \tag{3}$$

The boundary conditions are:

$$\mathbf{u} = \hat{\mathbf{u}} \quad \text{on } A_u; \qquad \boldsymbol{\sigma}\cdot\mathbf{n} = \boldsymbol{\Phi} \quad \text{on } A_\Phi \tag{3a}$$

where prescribed displacements $\hat{\mathbf{u}}$ on boundary surface portion A_u, and boundary surface tractions $\boldsymbol{\Phi}$ on portion A_Φ define a quasi-static boundary value problem. The rate representation of total strain in this elastic-visco-plastic model is given by

$$\dot{\boldsymbol{\varepsilon}} = \dot{\boldsymbol{\varepsilon}}_{\text{el}} + \dot{\boldsymbol{\varepsilon}}_{\text{ie}} + \dot{\boldsymbol{\varepsilon}}_{\text{th}} \tag{4}$$

where $\dot{\boldsymbol{\varepsilon}}_{\text{el}}, \dot{\boldsymbol{\varepsilon}}_{\text{ie}}, \dot{\boldsymbol{\varepsilon}}_{\text{th}}$ are the elastic, inelastic (plastic + creep), and thermal strain rate tensors, respectively. Stress rate $\dot{\boldsymbol{\sigma}}$ depends on elastic strain rate, and for a linear isotropic material with negligible large rotations, is given by Eq. (5) in which ":" represents inner tensor product.

$$\dot{\boldsymbol{\sigma}} = \underline{\underline{\mathbf{D}}} : (\dot{\boldsymbol{\varepsilon}} - \dot{\boldsymbol{\varepsilon}}_{\text{ie}} - \dot{\boldsymbol{\varepsilon}}_{\text{th}}) \tag{5}$$

$\underline{\underline{\mathbf{D}}}$ is the fourth order isotropic elasticity tensor given by Eq. (6):

$$\underline{\underline{\mathbf{D}}} = 2\mu\underline{\underline{\mathbf{I}}} + \left(k_{\text{B}} - \frac{2}{3}\mu\right)\mathbf{I}\otimes\mathbf{I} \tag{6}$$

Here μ and k_{B} are the shear modulus and bulk modulus, respectively, and are in general functions of temperature, while $\underline{\underline{\mathbf{I}}}$, $\mathbf{I}$ are fourth and second order identity tensors and "$\otimes$" denotes outer tensor product.

3.1. *Visco-plastic strain models*

Visco-plastic strain includes both strain-rate independent plasticity and time dependant creep. Creep is significant at the high temperatures of the solidification processes and is indistinguishable from plastic strain (Li and Thomas, 2005). Kozlowski et al. (1992) proposed a unified formulation with the following functional form to relate inelastic strain to stress, temperature, strain rate, and carbon content in the austenite phase of steel:

$$\dot{\bar{\varepsilon}}_{\text{ie}} = f(\bar{\sigma}, T, \bar{\varepsilon}_{\text{ie}}, \%\text{C}) \tag{7}$$

the equivalent inelastic strain-rate $\dot{\bar{\varepsilon}}_{\text{ie}}$ is a function of equivalent stress $\bar{\boldsymbol{\sigma}}$, temperature T, equivalent inelastic strain $\bar{\dot{\varepsilon}}_{\text{ie}}$, and steel grade defined by its carbon content %C:

$$\bar{\boldsymbol{\sigma}} = \sqrt{\frac{3}{2}\boldsymbol{\sigma}'_{\text{ij}}\boldsymbol{\sigma}'_{\text{ij}}} \tag{8}$$

$\boldsymbol{\sigma}'$ is a deviatoric stress tensor defined in Eq. (9):

$$\sigma'_{\text{ij}} = \sigma_{\text{ij}} - \frac{1}{3}\sigma_{\text{kk}}\delta_{\text{ij}} \tag{9}$$

The particular model below was chosen to match tensile test measurements of Wray (1982) and creep test data of Suzuki et al. (1988) for plain carbon steel in the austenite phase:

$$\dot{\bar{\varepsilon}}_{\text{ie}} = f_{\text{C}}(\bar{\sigma} - f_1\bar{\varepsilon}_{\text{ie}}|\bar{\varepsilon}_{\text{ie}}|^{f2-1})^{f3}\exp\left(-\frac{\text{Q}}{T}\right), \quad \text{where} \quad \text{Q} = 44,465,$$

$$f_1 = 130.5 - 5.128\times10^{-3}T, \quad f_2 = -0.6289 + 1.114\times10^{-3}T,$$

$$f_3 = 8.132 - 1.54\times10^{-3}T,$$

$$f_{\text{C}} = 46,550 + 71,400(\%\text{C}) + 12,000\ (\%\text{C})^2 \tag{10}$$

Q is activation constant, and f_1, f_2, f_3, f_{C}, are empirical functions of temperature or steel-grade, equivalent stress $\bar{\boldsymbol{\sigma}}$ is given in MPa, and temperature T in K.

To simulate the delta-ferrite phase of steel, a power-law constitutive model, was proposed by Zhu (1993) which generates the much higher creep rates experienced in this body-centered cubic phase, relative to the strong, face-centered cubic austenite phase. This constitutive model, given in Eq. (10a) was based on tensile test measurements by Wray (1976). It is applied in the solid whenever the volume fraction of ferrite is more than 10%. Otherwise, Eq. (10) is applied. This simple rule was preferred over a mixture rule based on phase fraction, because creep in the delta-ferrite phase dominates the mechanical behavior if this phase is continuous. The volume fractions of each phase are calculated from an iron–carbon phase diagram adjusted for other alloying components (1.52% Mn, 0.34% Si, 0.015% S, and 0.012% P), as implemented in the in-house code, CON2D (Li and Thomas, 2005):

$$\dot{\bar{\varepsilon}}_{\text{ie}} = 0.1\left|\frac{\bar{\sigma}}{f_{\delta\text{C}}(T/300)^{-5.52}(1+1000\bar{\varepsilon}_{\text{ie}})^m}\right|^n,$$

$$\text{where} \quad f_{\delta\text{C}} = 1.3678\times10^4(\%\text{C})^{-5.56\times10^{-2}},$$

$$m = -9.4156\times10^{-5}T + 0.3495,$$

$$n = \frac{1}{1.617\times10^{-4}T - 0.06166} \tag{10a}$$

Again equivalent stress $\bar{\sigma}$ is given in MPa, and temperature T in K in Eq. (10a).

A different visco-plastic model for steel at high temperature was proposed by Anand (1982) and Brown et al. (1989). Like the Kozlowski model, there is no explicit yield surface, as the instantaneous material response depends only on its current state. A single scalar variable s, called the deformation resistance, is used to represent the isotropic resistance to inelastic strain. The constitutive equation is given in Eq. (11):

$$\dot{\bar{\varepsilon}}_{\text{ie}} = A_{\text{A}}\exp\left(-\frac{\text{Q}_{\text{A}}}{T}\right)\left[\sinh\left(\xi\frac{\bar{\sigma}}{s}\right)\right]^{1/m} \tag{11}$$

The evolution equations for s are

$$\dot{s} = \left(h_0\left|1 - \frac{s}{s^*}\right|^a \text{sign}\left(1 - \frac{s}{s^*}\right)\right)\dot{\bar{\varepsilon}}_{\text{ie}} \tag{12}$$

with

$$s^* = \tilde{s}\left[\frac{\dot{\bar{\varepsilon}}_{\text{ie}}}{A_{\text{A}}}\exp\left(\frac{\text{Q}_{\text{A}}}{T}\right)\right]^n \tag{13}$$

Table 1 – Parameters used in the Anand material model for 1030 steel

Parameter	Value
s_o (MPa)	43
Q_A (K)	32514
A	1.E11
ξ	1.15
m	0.147
h_o (MPa)	1329
$\tilde{s}$ (MPa)	147.6
n	0.06869
a	1

where s is the deformation resistance (Pa), Q_A the activation energy over gas constant for Anand's material (K), A_A the pre-exponential factor (s^{-1}), ξ the multiplier of stress, m the strain rate sensitivity of stress, h_o the hardening/softening constant (Pa), $\tilde{s}$ the saturation value for s (Pa), n the strain rate sensitivity of saturation, and a is the strain rate sensitivity of hardening or softening.

In addition, an initial value for deformation resistance s_o must be defined.

Using the experimental data of Wray (1982) and Anand (1982) estimated the parameters for carbon steel in a carbon content range 0.05–0.5%C. The current Anand model implemented in ANSYS has been slightly modified from the original with the addition of a hyperbolic sine functional form of the constitutive equation and exponential hardening behavior. The standard material constants used for this model in this work are listed in Table 1. Brown et al. (1989) proposed the initial value for deformation resistance s_o to depend on temperature, while the initial work of Anand (1982) defined s_o to vary in the range of 35–52 MPa, depending on both temperature and strain rate. No temperature or composition dependence of any of these model parameters is currently available in ANSYS, so the average value of 43 MPa is chosen for s_o following the work of Huespe et al. (2000).

The Kozlowski model, on the other hand, has no adjustable parameters. For lower-carbon steels involving delta-ferrite, however, the Kozlowski model for austenite should be combined with a separate power law Eq. (10a) for temperatures at which delta-ferrite is present. Details of the complete phase-dependent constitutive equations are given elsewhere (Zhu, 1993; Lush et al., 1989).

The steels considered in this work are assumed to harden isotropically, so the von Mises loading surface, associated plasticity, and normality hypothesis of the Prandtl–Reuss flow law, Eq. (14) (Mendelson, 1983) is used to calculate visco-plastic strain components:

$$(\dot{\varepsilon}_{ie})_{ij} = \frac{3}{2}\dot{\varepsilon}_{ie}\frac{\sigma'_{ij}}{\tilde{\sigma}} \tag{14}$$

3.2. *Thermal strain*

Thermal strains ε_{th} arise due to volume changes caused by both temperature differences and phase transformations, including solidification and solid-state phase changes between crystal structures, such as austenite and ferrite:

$$(\varepsilon_{th})_{ij} = \int_{T_0}^{T} \alpha(T)\,dT\delta_{ij} \tag{15}$$

where α is the temperature dependant coefficient of thermal expansion, T_0 an important reference temperature and δ_{ij} is Kronecker's delta. The choice of T_0 is arbitrary, but it significantly affects the associated α function.

4. Local Time Integration of the inelastic constitutive models

Owing to the highly strain-dependant inelastic responses, a robust integration scheme is required to integrate either the Kozlowski or Anand equations over a generic time increment Δt. The system of ordinary differential equations defined at each material point by the Kozlowski model Eq. (10) or the Zhu power law model Eq. (10a) is converted into two "integrated" scalar equations by the Euler backward method and then solved using a special bounded Newton–Raphson method (Zhu, 1993; Koric and Thomas, 2006; Lush et al., 1989). Details of this local integration scheme can be found at Zhu (1993), Koric and Thomas (2006) and Lush et al. (1989) along with the derivation of the Jacobian consistent with this method.

Similarly, ANSYS uses the Euler-backward scheme to integrate Eqs. (11) and (12) (ANSYS Inc., 2006). The details of this local integration scheme that is built into ANSYS and specially optimized for the Anand model are not publicly available.

The solution obtained from this "local" integration step from all material (gauss) points is used to update the global finite-element equilibrium equations, which are solved using the Newton–Raphson based nonlinear finite-element procedures in ABAQUS or ANSYS (ABAQUS Inc., 2006; ANSYS Inc., 2006).

5. Comparison of constitutive models with experimental data

The two constitutive models were first evaluated for spatially uniform conditions, by simply integrating the equations with a local method. Fig. 1 compares the calculated tensile curves with experimental data of Wray (1982) for different carbon contents. The Kozlowski model correctly captures the slight softening effect of increasing carbon content for this fully austenitic condition. Lacking any dependency on steel grade, the Anand model is represented with a single curve, which underestimates stress for the low and mild carbon content steels, and underestimates work hardening, as indicated by the flatness of the curves.

Fig. 2 compares the stresses at 5 pct strain measured by Wray (1976) at different temperatures to those predicted with the Kozlowski austenite model or Zhu power law for delta-ferrite and the Anand model. Both model systems exhibit the correct drop in stress when integrated at lower constant strain rate. The experiments and Kozlowski/Zhu model predictions in this figure both show that delta-ferrite, which forms in low carbon steels at higher temperatures, is much weaker than

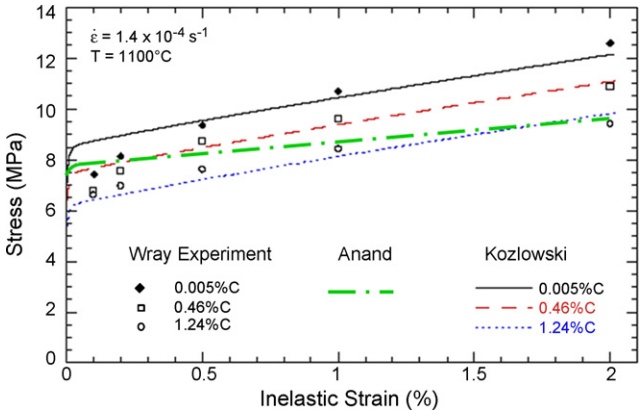

Fig. 1 – Tensile stress curves calculated with Kozlowski and Anand models for various carbon content and compared to Wray experimental data.

austenite. This important effect of phase explains the lower stress measured in ferritic Si-steel at lower temperature, while the ultra-low carbon steel and Si-steel show similar stresses in the fully ferritic region above 1400 °C. The Anand model fails to capture this significant change in mechanical behavior of low carbon steel shells containing delta-ferrite.

For the 1030 steel, Huespe et al. (2000) showed that the Kozlowski model has a generally better fit with available experimental data of Suzuki et al. (1988), while the Anand model showed a slightly better agreement with experimental data of Wray (1982). However, due to the uncertainty of s_o and lack of dependency on carbon content %C in the Anand model, it was concluded in that work that the Kozlowski model is better. A recent survey of various constitutive models of steel at elevated temperature conducted by Pierer et al. (2005) has found that the Kozlowski model produces the closest match with experimental steel solidification force–elongation curves. Additional information on these models, including further comparison with experimental measurements can be found in the following papers: Kozlowski et al. (1992), Anand (1982), Brown et al. (1989), Huespe et al. (2000), Pierer et al. (2005) and Meng et al. (2004).

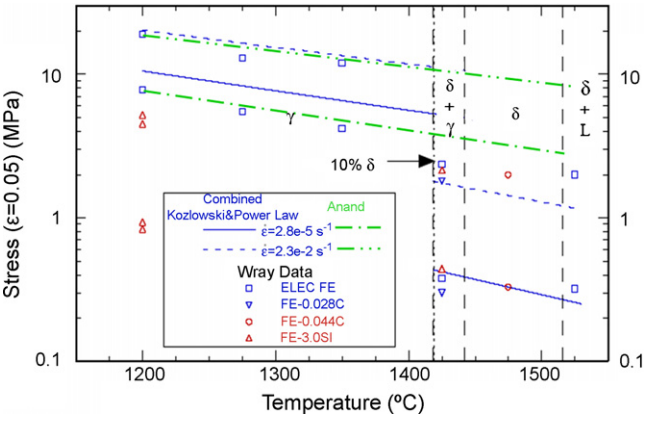

Fig. 2 – Constitutive model comparison with Wray experimental data for low carbon steel, showing mechanically weaker delta-ferrite phase.

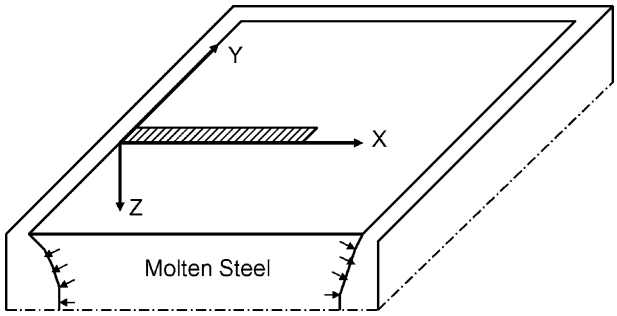

Fig. 3 – Solidifying slice.

6. Analysis of solidifying shell in continuous casting mold

In many solidification processes, such as the continuous casting of steel, one dimension of the casting is much longer than the others, and is otherwise unconstrained. In this case, it is quite reasonable to apply a condition of generalized plane strain in the long (axial) direction (z), and to solve a two-dimensional thermal stress problem in the transverse (x–y) plane. This condition reasonably allows a two-dimensional transient mechanical computation in the plane section to produce the complete three-dimensional stress state in the casting. While generalized-plane-strain elements are available in ABAQUS, the current implementation of so-called visco elements, which only works with Anand's material in ANSYS, does not support generalized plane strain. Therefore, this comparative investigation employs a simple plane-strain implementation in both codes.

The domain adopted for this problem is a thin slice through the shell thickness given in Fig. 3 with the casting condition listed in Table 2.

For the heat conduction computation, the high Peclet number ($V_c L\rho c_p/k$) associated with the high casting speed (V_c) and low thermal conductivity (k) of steel continuous casting makes axial conduction negligible relative to axial advection (Meng and Thomas, 2003; Li and Thomas, 2005). Thus, the same simple slice domain that moves with the strand in a Langrangian frame of reference can be used for both the heat transfer and mechanical computations. Fig. 4 shows the domain and boundary conditions for both models. An instantaneous interfacial heat flux profile that varies with time down the mold according to mold thermocouple measurements (Li

Table 2 – Casting conditions

Parameter	Value
Steel casting speed (m/min)	2.2
Working mold length (mm)	670
Carbon content	0.27%C
Initial temperature (°C)	1540
Liquidus temperature (°C)	1500.70
Solidus temperature (°C)	1411.79
Ref. temperature for thermal expansion (°C)	1540
Density (kg/m^3)	7400
Poisson's ratio	0.3

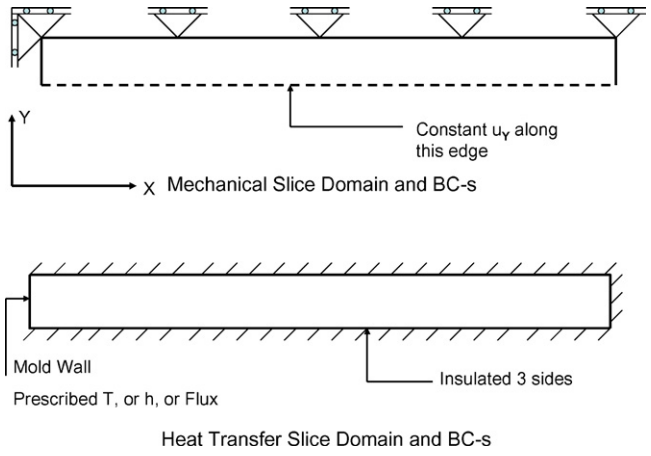

Fig. 4 – Mechanical and thermal finite element domains.

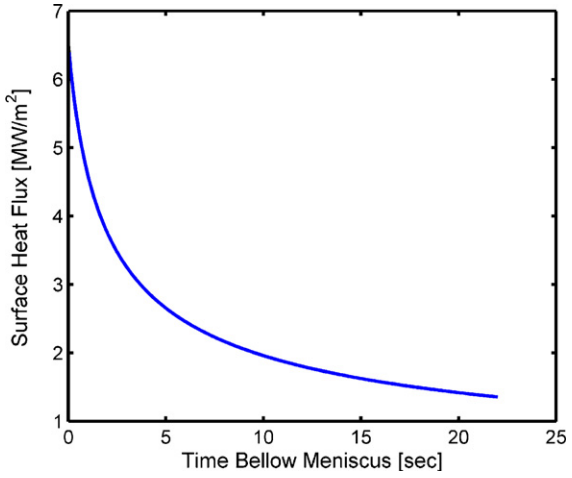

Fig. 5 – Instantaneous interfacial heat flux.

and Thomas, 2005) is given in Fig. 5, and is applied at the left edge of the domain. Due to the large width (x) of the casting compared to the thickness (y) of this simple domain, a second generalized plane strain state is applied in the y direction. This condition was imposed by coupling the displacements of all nodes along the bottom edge of the slice domain. This was accomplished using the *EQUATION option in ABAQUS (ABAQUS Inc., 2006), and the CP command in ANSYS (ANSYS Inc., 2006). The normal (x) displacement of all nodes along the bottom edge of the domain is fixed to zero. Tangential stress was left equal zero along all surfaces. Finally, the ends of the domain are constrained to remain vertical, which prevents any bending in the xy plane.

Temperature-dependent properties were chosen for 0.27%C plain mild-carbon steel with $T_{sol} = 1411.79\,^{\circ}C$ and $T_{liq} = 1500.72\,^{\circ}C$ (solidus and liquids temperatures). The enthalpy curve used to relate heat content and temperature in this study, $H(T)$, is shown in Fig. 6. It was obtained by integrating the specific heat curve fitted from measured data of Pehlke et al. (1982). While this enthalpy data is input directly into ANSYS, ABAQUS tracks the latent heat $Hf = 257{,}867\,J/kg$ separately from the specific heat c_p, which is found from the slope of this H curve, except in the solidification region, where

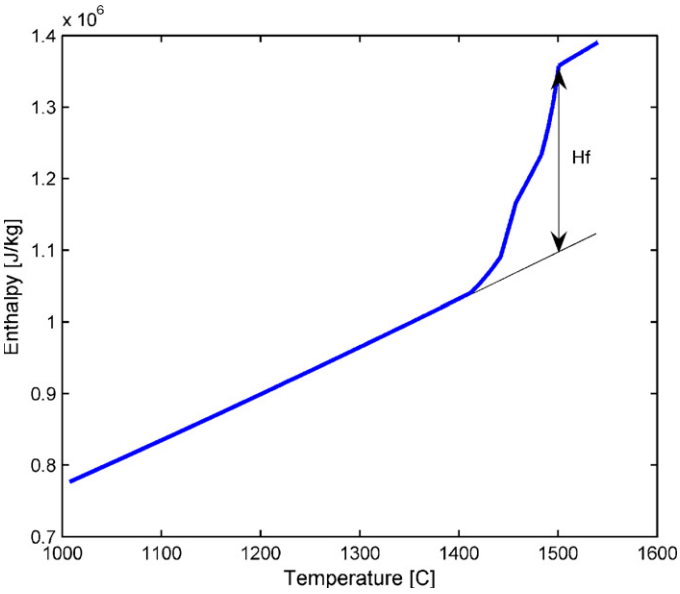

Fig. 6 – Enthalpy for 0.27%C plain carbon steel.

c_p is found from Lewis et al. (1996) as follows:

$$c_p = \frac{dH}{dT} - \frac{Hf}{(T_{liq} - T_{sol})} \tag{16}$$

The temperature dependent conductivity function for 0.27%C plain carbon steel is fitted from data measured by Harste (1989), and is given in Fig. 7. The conductivity increases in the liquid region by a factor of 6.65 to partly account for the effect of convection due to flow in the liquid steel pool (Huang et al., 1992). Density was assumed constant at this work, 7400 kg/m^3, in order to maintain constant mass.

The temperature-dependant coefficient of thermal expansion $\alpha(T)$ is calculated from the thermal linear expansion function TLE (Li and Thomas, 2005) with a reference tempera-

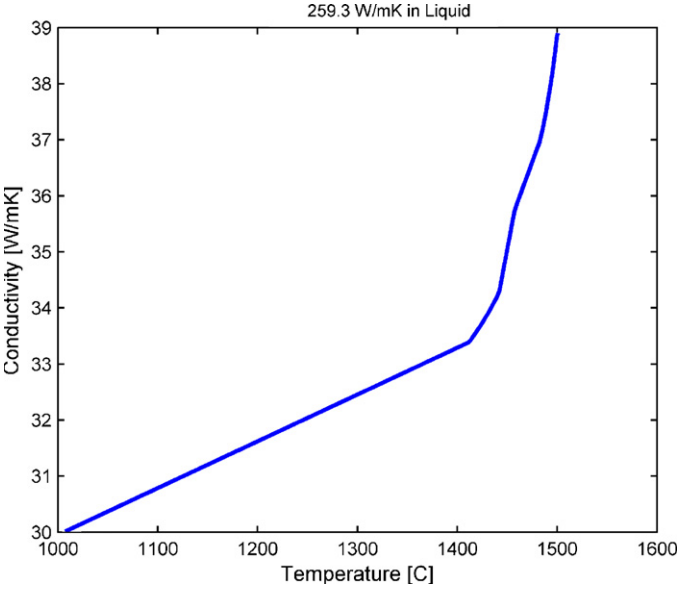

Fig. 7 – Thermal conductivity for 0.27%C plain carbon steel.

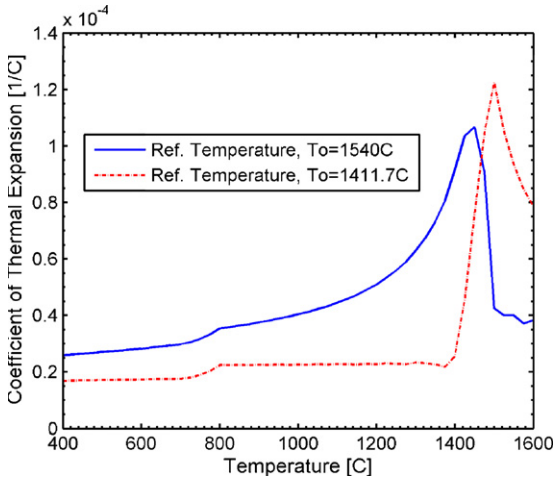

Fig. 8 – Coefficient of thermal linear expansion for 0.27%C plain carbon steel, reference temperatures: $T_0 = 1540$ and 1411.7 °C.

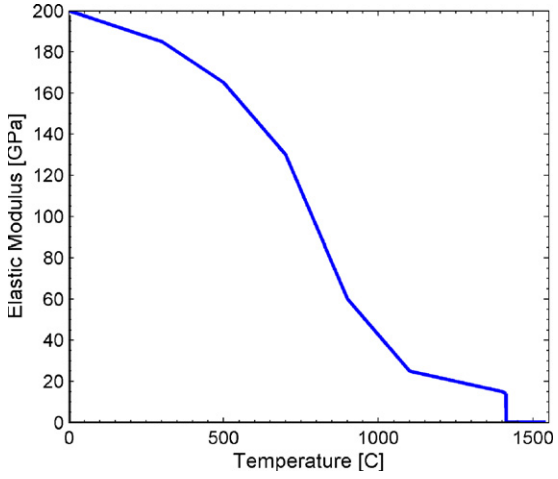

Fig. 9 – Elastic modulus for plain carbon steel.

ture of $T_0 = 1540$ °C, and is given in Fig. 8. An alternative, exactly equivalent thermal-expansion function is included in this figure using a reference temperature of $T_0 = T_{sol} = 1411.79$ °C.

Poisson ratio is 0.3 constant. Elastic modulus E generally decreases as the temperature increases, although its value at very high temperatures is uncertain. The temperature-dependent elastic modulus curve used in this model was fitted from measurements from Mizukami et al. (1977), as shown in Fig. 9. The liquid and mushy zone is modeled by lowering elastic modulus by three orders of magnitude. This method is easy to apply but cannot model the generation of inelastic strain and stress in the liquid/mushy zone which is crucial for hot tearing prediction (Li and Thomas, 2005). It also sometimes introduces a numerical ill conditioning of the global stiffness matrix after finite-element assembly which might be a problem for sparse linear solvers. Other more sophisticated liquid/mushy models have been proposed by Zhu (1993), Li and Thomas (2005), and Koric and Thomas (2006).

A 20 s simulation was performed, which corresponds to a 670 mm long shell of steel cast at a casting speed of 2 m/min. The heat transfer analysis is run first to get the temporal and

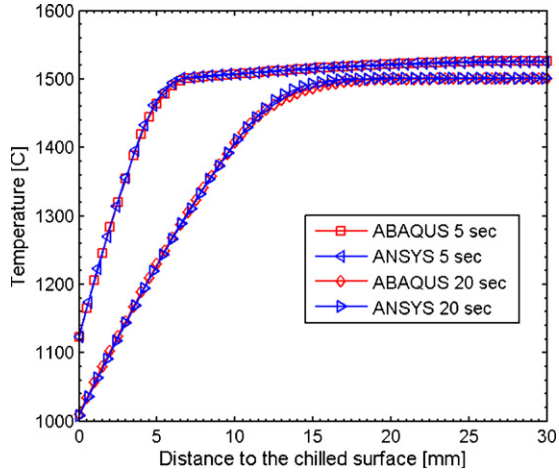

Fig. 10 – Temperature distribution along the solidifying slice in continuous casting mold.

spatial temperature field. Stress analysis is then run using this temperature field. The domain used in both codes has a single row of 300 plane 4-node elements in both thermal and stress analysis. A formal study of mesh and time increment refinement was conducted by Zhu (1993), which shows that the 300-node mesh used here is more than sufficient to achieve accuracy within 1% error with a fixed time increment of 0.01 s (1000 time increments per 10 s) compared to the analytical solidification solution for the elastic-perfectly plastic material (Weiner and Boley, 1963).

7. Results and discussion

The temperature results predicted with ABAQUS and ANSYS are in excellent agreement, as shown in Figs. 10 and 11. Considering that the two codes employ different forms of thermal parameters (H and k in ANSYS; T_{sol}, T_{liq}, Hf, and k in ABAQUS), this shows that both sets of thermal material properties are consistent. Furthermore, the two numerical implementations are equivalent.

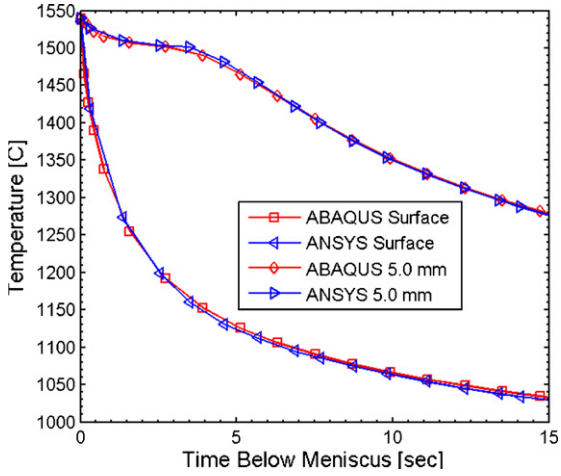

Fig. 11 – Temperature history for the surface material point and the material point 5 mm from the surface.

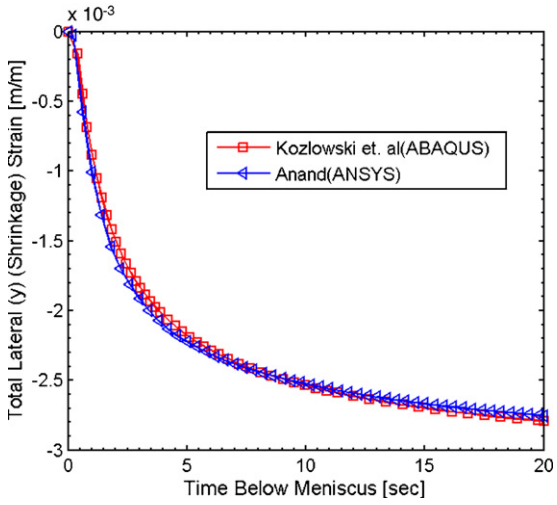

Fig. 12 – Lateral shrinkage history of the bottom edge nodes.

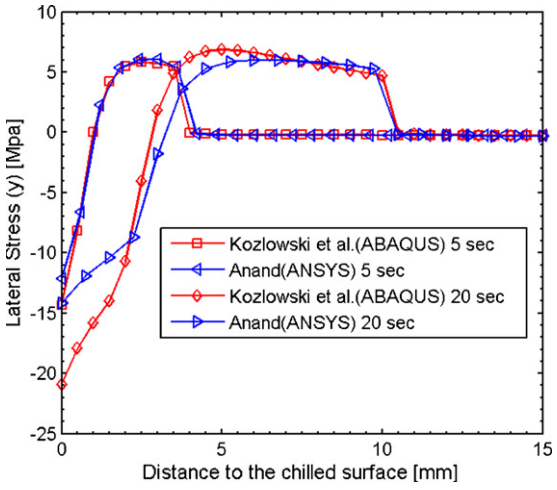

Fig. 13 – Lateral (y) stress distribution along the solidifying slice in continuous casting mold.

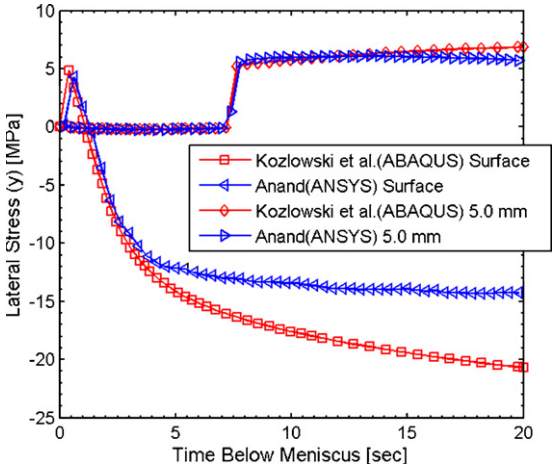

Fig. 14 – Lateral (y) stress history for the surface material point and the material point 5 mm from the surface.

The temperature gradient through the shell is almost linear from near the solidification front to the cooled surface and it gradually drops as solidification proceeds. The typical cooling histories for two material points in Fig. 11 each show the classic drop in cooling rate as each point beneath the surfaces passes through the "mushy region" between the solidus and liquidus temperatures. The solidification front grows roughly parabolically with time, which matches both theoretical expectations and plant measurements (Meng and Thomas, 2003).

The total lateral (y) shrinkage strain history given in Fig. 12 for the bottom edge nodes also shows a very good agreement between two models. This shrinkage displacement is the same across the entire domain, and shows the decrease in the average width of the solidifying shell, which is accommodated in practice by tapering the mold walls. This result represents a prediction of ideal taper, and shows that more taper is needed near the beginning of solidification in the top region of the mold. This calculation is relatively insensitive to the constitutive model, because the shrinkage is predominantly thermal strain, and can be reasonably approximated by simple thermal strain calculations (Thomas and Ojeda, 2003).

The stress predictions, given in Figs. 13 and 14 match reasonably well at early times, but start to diverge with increasing time. For both models, the faster cooling of the interior relative to the surface region naturally causes interior contraction and tensile stress, which is offset by compression at the surface. The Anand model underpredicts both the compressive surface stress and the internal tensile peak. This finding is consistent with the stress underprediction from Fig. 1 as well as with the axial stress results from the in-house code of Huespe et al. (2000) for round billet casting under different conditions. These results indicate the earlier observed differences between the two constitutive models, which increase with decreasing temperature. Qualitatively, however, both models reasonably predict thermal–mechanical behavior during solidification, and can provide insights into casting processes.

Finally, the wall clock times of the two codes in this work are comparable. The Anand model with ANSYS was faster, taking 3.5 min, versus 5.5 min for the Kozlowski/Zhu model with ABAQUS. Both simulations were performed on the IBM p690 platform with a Power 4, 1.3 GHz CPU.

8. Conclusions

Temperature and stress in a solidifying slice through a realistic steel continuous caster are predicted with two different elastic-visco-plastic constitutive laws for plain-carbon steel using two commercial finite-element programs. The Anand law is integrated by the Euler-Backward method built into ANSYS. The results are compared with the Kozlowski model for austenite combined with the Zhu power-law model for delta-ferrite, integrated in ABAQUS with a local-global integration scheme implemented via a user-defined UMAT subroutine.

While the temperature and total strain results are in excellent agreement, the Anand model under-predicts the peak stresses in both compression and tension. The results are consistent with the tensile stress comparisons in Fig. 1 as well as

the findings of previous work (Huespe et al., 2000) using an in-house code. The Anand model with ANSYS qualitatively predicts the expected thermal–mechanical behavior with the least CPU time. However, the Kozlowski/Zhu model has been validated with experimental measurements, accurately incorporates steel grade dependency, needs no adjustable parameters to be defined, and can utilize the generalized plane-strain condition in ABAQUS. In addition, only the Kozlowski/Zhu model correctly predicts the weakening behavior of delta-ferrite, which forms near the solidification front in low carbon steels.

In conclusion, both ANSYS and ABAQUS enable modeling of complex realistic casting phenomena including variable interfacial gap heat transfer, ferrostatic pressure from the liquid, thermo-mechanical contact between the mold and strand, mold taper, and complex three-dimensional geometric features. Two efficient and convenient approaches are available to investigate thermal–mechanical behavior involving the solidification of steel, especially while in the austenite phase.

Acknowledgement

The authors would like to thank the National Center for Supercomputing Applications (NCSA) at the University of Illinois for providing computing and software facilities.

REFERENCES

ABAQUS Inc., 2006. User Manuals v6.6.

Anand, L., 1982. Constitutive equations for the rate dependant deformation of metals at elevated temperatures. ASME J. Eng. Mater. Technol. 104, 12–17.

ANSYS Inc., 2006. User Manuals v100.

Boehmer, J.R., Funk, G., Jordan, M., Fett, F.N., 1998. Strategies for coupled analysis of thermal strain history during continuous solidification processes. Adv. Eng. Software 29 (7–9), 679–697.

Brown, S.B., Kim, K.H., Anand, L., 1989. An internal variable constitutive model for hot working of metals. Int. J. Plasticity 6, 95–130.

Farup, I., Mo, A., 2000. Two-phase modeling of mushy zone parameters associated with hot tearing. Metall. Mater. Trans. 31, 1461–1472.

Grill, A., Brimacombe, J.K., Weinberg, F., 1976. Mathematical analysis of stress in continuous casting of steel. Ironmaking Steelmaking 3, 38–47.

Harste, K., 1989. Investigation of the shrinkage and the origin of mechanical tension during solidification and successive cooling of cylindrical bars of Fe–C alloys. Ph.D. Thesis. Technical University of Clausthal.

Huang, X., Thomas, B.G., Najjar, F.M., 1992. Modeling superheat removal during continuous casting of steel slabs. Metall. Trans. B 23B, 339–356.

Huespe, A.E., Cardona, A., Nigro, N., Fachinotti, V., 2000. Visco-plastic constitutive models of steel at high temperature. J. Mater. Process. Technol. 102, 143–152.

Koric, S., Thomas, B.G., 2006. Efficient thermo-mechanical model for solidification processes. Int. J. Num. Meth. Eng. 66, 1955–1989.

Koric, S., Thomas, B.G., 2007. Thermo-mechanical model of solidification processes with ABAQUS. In: ABAQUS Users Conference 2007, Paris, France, May 20–22, pp. 320–336.

Koric, S., Thomas, B.G., Xu, K, Spangler, C., 2007. Coupled thermo-mechanical model of steel beam blanks. Part I. Model formulation and validation, Metall. Mater. Trans. B (2007), in review.

Kozlowski, P.F., Thomas, B.G., Azzi, J.A., Wang, H., 1992. Simple constitutive equations for steel at high temperature. Metall. Trans. 23A, 903–918.

Kristiansson, J.O., 1984. Thermomechanical behavior of the solidifying shell within continuous casting billet molds—a numerical approach. J. Therm. Stresses 7, 209–226.

Lewis, R.W., Morgan, K., Thomas, H.R., Seetharamu, K.N., 1996. The Finite Element Method in Heat Transfer Analysis. Wiley, New York.

Li, C., Thomas, B.G., 2002a. Analysis of the potential productivity of continuous cast molds. In: Irons, G., Cramb, A. (Eds.), Brimacombe Memorial Symposium. Vancouver, Canada. Canadian Inst. Min. Metall., Montreal, Canada, pp. 595–611.

Li, C., Thomas, B.G., 2002b. Maximum casting speed for continuous cast steel billets based on sub-mold bulging computation. In: Steelmaking Conf. Proc., Vol. 85, ISS, Warrendale, PA, Nashville, TN, March 10–13, pp. 109–130.

Li, C., Thomas, B.G., 2005. Thermo-mechanical finite-element model of shell behavior in continuous casting of steel. Met. Mater. Trans. B 35B (6), 1151–1172.

Lush, A.M., Weber, G., Anand, L., 1989. An implicit time–integration procedure for a set of integral variable constitutive equations for isotropic elasto-viscoplasticity. Int. J. Plasticity 5, 521–549.

Mase, G.E., Mase, G.T., 1999. Continuum Mechanics for Engineers, 2nd ed. CRC Press.

Mendelson, A., 1983. Plasticity: Theory and Applications. Krieger Publ. Co.

Meng, Y., Thomas, B.G., 2003. Heat transfer and solidification model of continuous slab casting: CON1D. Metall. Mater. Trans. 34B, 685–705.

Meng, Y., Li, C., Parkman, J., Thomas, B.G., 2004. Simulation of shrinkage and stress in solidifying steel shells of different grades. In: Rappaz, M. (Ed.), A Symposium in Honor of Wilfried Kurz. TMS, Charlotte NC, March 15–18, pp. 33–39.

Mizukami, H., Murakami, K., Miyashita, Y., 1977. Elastic modulus of steels at high temperature. J. Iron Steel Inst. Jpn. 63 (146), S-652.

Morgan, K., Lewis, R.W., Williams, J.R., 1978. Thermal Stress Analysis of A Novel Continuous Casting Process. The Mathematics of Finite Elements and its Applications, vol. 3. Academic Press.

Pehlke, R.D., Jeyarajan, A., Wada, H., 1982. Summary of thermal properties for casting alloys and mold materials. Report No. NSF/MEA-82028. Department of Materials and Metallurgical Engineering, University of Michigan.

Pierer, R., Bernhard, C., Chimani, C., 2005. Evaluation of common constitutive equations for solidifying steel. BHM 150, 163–169.

Rammerstrofer, F.G., Jaquemar, C., Fischer, D.F., Wiesinger, H., 1979. Temperature Fields, Solidification Progress and Stress Development in the Strand During A Continuous Casting Process of Steel, Numerical Methods in Thermal Problems. Pineridge Press, pp. 712–722.

Risso, J.M., Huespe, A.E., Cardona, A., 2006. Thermal stress evaluation in the steel continuous casting process. Int. J. Num. Meth. Eng. 65 (9), 1355–1377.

Suzuki, T., Take, K.H., Wunnenberg, K., Schwerdtfeger, K., 1988. Creep properties of steel at continuous casting temperatures. Ironmaking Steelmaking 15, 90–100.

Thomas, B.G., Ojeda, C., 2003. Ideal taper prediction for slab casting. In: Manfred Wolf Memorial Symposium Proceedings, ISS-AIME, Warrendale, PA, pp. 295–308.

Thomas, B.G., Brimacombe, J.K., Samarasekera, I.V., 1986. The formation of panel cracks in steel ingots, a state of the art review, hot ductility of steel. Trans. Iron Steel Soc. 7, 7–20.

Weiner, J.H., Boley, B.A., 1963. Elastic–plastic thermal stresses in a solidifying body. J. Mech. Phys. Solids 11, 145–154.
Wimmer, F., Thone, H., Lindorfer, B., 1996. Thermomechanically-coupled analysis of the steel solidification process in continuous casting mold. In: ABAQUS Users Conference.
Wray, P.J., 1976. Plastic deformation of delta-ferritic iron at intermediate strain rates. Metall. Trans. A 7A, 1621–1627.
Wray, P.J., 1982. Effect of carbon content on the plastic flow of plain carbon steel at elevated temperatures. Metall. Trans. A 13, 125–134.
Zhu, H., 1993. Coupled thermal–mechanical finite-element model with application to initial solidification. Ph.D. Thesis. University of Illinois.